Theoretical and experimental investigation of a servo control's dynamic stiffness and smoothness

Alexander Baehr, Peter Mutschler *Member IEEE*
Darmstadt University of Technology, Department of Power Electronics and Control of Drives
Landgraf-Georg-Str. 4, 64283 Darmstadt, Germany
abaehr@srt.tu-darmstadt.de

***Abstract*— This paper summarizes a comparison of speed computation methods for servo control, regarding their influence on controller performance. In addition, state control is taken into account as a means for actively damping mechanical resonance. The effects of sensor quality and control timing are discussed. The theoretical background is investigated and compared to the measurements.**

***Index Terms*— servo control, state control, direct drive, resonant system, three inertia system, observer, stiffness, smoothness**

I. Introduction

This paper investigates schemes to control a 2.2 kW servo motor plant. The experimental setup and control structure are described in section II, a simulation model in section III.

A theoretical investigation about the relationship between controller gain and dynamic stiffness has been published in [1]. Stiff direct drives are considered that use the usual cascade of position, speed and current controllers (fig. 1). Two approximate equations are developed that yield the dynamic stiffness for given control parameters. In section IV, the considerations are extended, taking into account the delay of speed acquisition. Section V shows the relationship between controller gain and speed quality, using experimental results.

Section VII shows the achievable control performance with P/PI cascade controllers, using different methods to compute the actual speed signal. A discussion of the methods and part of the results has been published in [2]. The best performance in relation to design effort have been achieved using differentiating low-pass filters, low-pass & notch combinations, and observers modeling the resonant behavior of the setup as a two or three inertia resonant system. Section VIII adds results achieved with a more precise encoder, Section IX discusses the aspect of controller timing.

Section X discusses active damping of the mechanical resonance using state controllers. To design a state controller, two methods are well known: pole placing or linear-quadratic controller design. Goslar [3] suggests pole placing using the path of minimum pole sensitivity, i. e. where the resonant poles can be moved leftward with the norm of the feedback vector increasing as few as possible. The resulting path is directly leftward, i. e. keeping the pole's imaginary part constant. This result was confirmed for the setup regarded here. Fassnacht [4] suggests a linear-quadratic controller. Only the main diagonal of the weighting matrix is filled with values different from zero, which are developed by try-and-error.

Control performance is measured in this paper on the one hand as the r.m.s. deviation of the speed signal during speed control at constant reference speed and no load. For an ideal controller, the speed would be exactly constant, so its r.m.s. deviation is a measure for the non-ideality of the control loop. It is calculated by off-line time discrete derivation record of the encoder position signal, so the data regarded are not smoothed by the respective filter or observer.

To make comparison easier, all control loops were tuned to an equal steady-state behavior, i. e. such that the r.m.s. deviation was equal. This was done by varying the delay time constant of the speed acquisition filter or observer and the controller gain. The speed deviation goal was 0.1 rad/s for the 2048-line encoder and 0.7 rad/s for the 5000-line encoder; subtracting the different imprecisions, this means an equal deviation in fact (see section II).

On the other hand, performance is measured regarding the load step rejection with P-position- / PI-speed-control. Several defined stepwise load torque changes of amount ΔT were executed by the load machine, and the maximum deviation $\Delta\theta$ from the reference position was used to compute the dynamic stiffness of the control loop C_{dyn} as

$$C_{dyn} = \frac{\Delta T}{\Delta \theta} \tag{1}$$

II. Experimental Setup and Control Design

The controls were tested on an experimental setup which consists mainly of two coupled 2.2 kW permanent magnet servo motors, two inverters with a coupled DC link, signal processing electronics, and a PC where the control algorithms are implemented. The drive's nominal torque is 4.3 Nm, the torque constant $k_T = 0.533$ Nm/A in the sense of fig. 7, the overall inertia of the setup is $J = 20.05$ kgcm^2. An incremental encoder and an acceleration sensor are mounted on a short extension sleeve at the controlled servo's second shaft end. Only the encoder signal is used here.

Two position encoders were tested on this setup: A Huebner HOGS80 with 2048 lines (bought in the year 2000), and a 5000-line Heidenhain ERN180 from 2002. Both provide an hollow shaft with 25mm diameter. The 2048-line encoder is fixed to the servo housing with a thin steel plate, causing additional oscillation in the frequency range around 1000 Hz. The speed error at zero speed (discrete derivative, no filter), which results only from encoder noise, is about 0.06 rad/s. The 5000-line encoder is fixed to the servo with a steel frame, causing

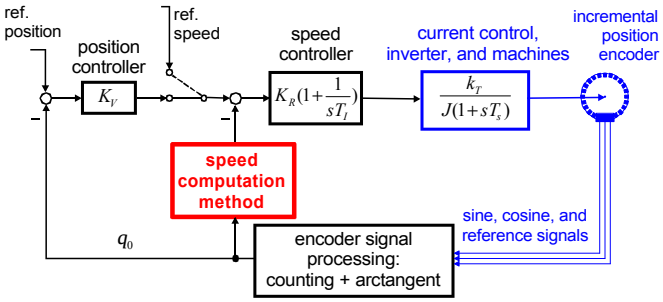

Fig. 1. Schematic of the control system

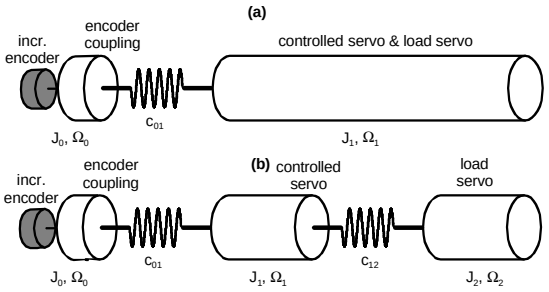

Fig. 2. Two and three mass models for the regarded setup

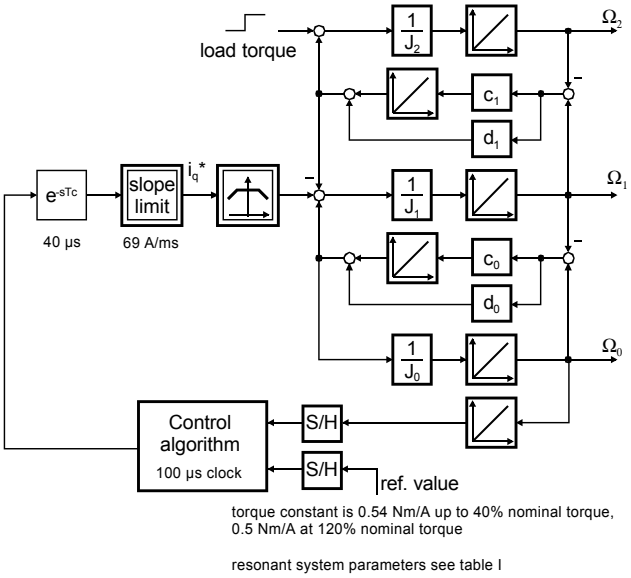

Fig. 3. Simulation model

no significant resonance. Its noise is very low, but the signals have large systematic errors [5] that would cause a speed error of 0.033 rad/s in the worst case. Thus, precision of both encoders is comparable, keeping in mind the different number of lines. The encoder signals are digitalized by 12-bit AD-converters; the overall precision of the electronics is ± 1 least significant bit. The position is then computed using a line counter for the coarse position and the arctangent equation for interpolation [6].

The load servo is used to simulate a mechanical load. Its inverter is switched off for smooth turning experiments, and run in current control mode to get quick load changes for the disturbance rejection experiments. However, its controller is rather slow; the response to a reference change is approximately a ramp function, reaching the new setpoint after 500 μs.

The structure of the used control system is shown in fig. 1: It is the usual cascade control. For the block "speed computation method", several filters and observers were tested; see sections VII ff. Either PI-speed control or P-position / PI-speed-control are implemented in the PC software for the controlled servo motor; the parameters depend on the speed computation method used. Current control is done by an analogue bang-bang controller working in the stationary reference frame [7].

The speed controller was designed according to the well-known symmetrical optimum, based on the load acquisition filter's or observer's delay time constant together with an additional time constant of $T_S = 234\ \mu$s for digital control and current control loop. When using the speed signal from an observer, the symmetrical optimum would have yielded too low controller gains if the observer's time constant is taken into account, and too high gains if not. Thus, an extension of the symmetrical optimum was used where the proportional gain is chosen arbitrarily, and the integral gain is computed such that in the bode plot, the maximum phase occurs at crossover frequency. For design of the position controller, the amplitude optimum was used every time. No further optimization of the control parameters was done in order to keep the results comparable with respect to the different speed acquisition methods.

III. Simulation Model

This paper relies on two different kinds of measurements: speed quality at steady state and dynamic stiffness against load changes. The speed quality is very hard to simulate, because the exact kind of noise in all system parts, model uncertainties, damping coefficients etc. need to be known very exactly. It was not possible to find a model that simulates the measured data correctly. The reaction to a load change, however, mainly depends on the system and control parameters and is therefore possible to simulate.

The most important feature of the setup is a nearly undamped mechanical resonance. The first two resonance frequencies were modeled using the three-inertia model shown in fig. 2(b). The encoder is mounted on a short extension sleeve at the controlled servo's opposite shaft end. The resonant system consisting of servo and sensor mass has a resonant frequency of about 900Hz. As opposed to many literature cases, this was found to be the most important resonance to handle. The drive and load form two with elastic coupling, which ist the source of the 2nd resonant frequency.

The mathematical model of the resonant system forms the main part of the simulation model shown in fig. 3. It consists of the three inertias J_0, J_1, J_2, two elastic couplings c_{01} and c_{12} with damping coefficients d_{01} and d_{12}.

The current control used in the experimental setup is an analog bang-bang controller, that keeps the current space vector in a specified area around the reference using

hysteresis comparators [7]. Any reference value change will be followed as fast as the DC link voltage and stator inductance allow it. This is approximated by a slope limit. Alternatively, the current control could be modeled more precisely using ideal comparators and a lookup table; the motor can be represented using the linear model in field-oriented reference frame. The effect of this augmentation was a small reduction of the simulated stiffness using high-gain controls, strongly depending on how the minimum turn-on time is implemented. As the simplified model works considerably faster and the difference in results is neglectable, it has been used.

The current-torque relationship is not exactly linear because of saturation in the stator back. It has been implemented in the simulation model as a static characteristic according to the motor's datasheet. This caused a reduction of the simulated stiffness with high controller gains.

The plant is simulated as a three-inertia system with light damping. However, since the three-inertia model that is used for observers does not mirror the static stiffness properly, an adapted model was used (see sections VI and VII).

Simulating the load servo's response function, the measured stiffness values could be reproduced within a tolerance of $\pm 7\%$. The stiffness of observer controls was simulated too low, while it was simulated too high for controls using a filter. The model will be used in the following to simulate the result of an ideal stepwise load change, since this is the exact definition of dynamic stiffness.

IV. Dynamic Stiffness vs. Controller Gain

A theoretical discussion of the relationship between controller parameters and dynamic stiffness was published by Weck and others [1]. It discusses the cascade control structure shown in fig. 1, neglecting the delays of current control loop and speed acquisition. Two approaches of the dynamic stiffness are derived analytically from the system's transfer function. The first one, neglecting the speed controller's integral part, yields the equation

$$C_{dyn} = K_V K_R k_T \tag{2}$$

This equation is far away from the experimental and simulation results (compare fig. 4(a) and (c)). The second approach fits the experimental results better; it takes into account the integral controller, but needs other neglections. The result becomes much more complex:

$$C_{dyn} = K \left(1 + \frac{e^{-D\frac{\pi}{\sqrt{1-D^2}}}}{\sqrt{1-D^2}} \right)^{-1} \tag{3}$$

$$\text{where } K = \frac{K_R k_T \left(1 + K_V T_I\right)}{T_I}$$

$$D = \frac{1}{2}\sqrt{\frac{K_R k_T T_I}{J\left(1 + K_V T_I\right)}}$$

Using high order observers, it seems necessary to regard the observer's considerable delay in detecting load changes. Unfortunately, it is no longer possible to solve the problem analytically. Instead, simulations

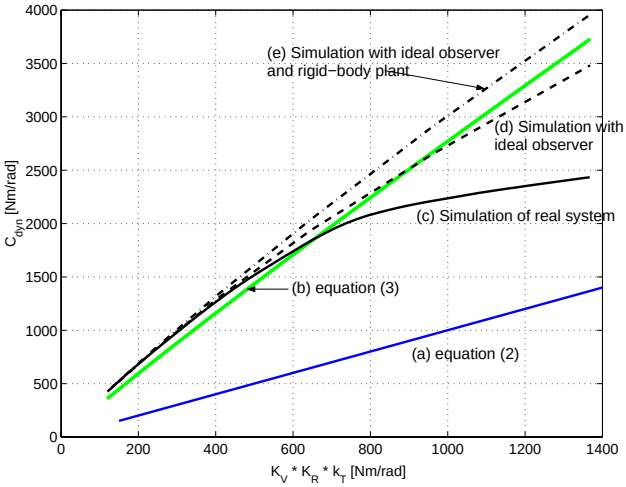

Fig. 4. Simulation and theoretical results for dynamic stiffness vs. controller gain

were carried out using different models. Fig. 4(c) shows results from a simulation of the three-inertia system, three-inertia observer, and different controller designs using extended symmetrical optimum and optimum of magnitude. Fig. 4(b) shows the results of equation (3). Except an imprecision in the lower lange, which is due to the neglections made in [1], the main difference is that for higher gains, (3) increases nearly linearly while the simulated controller gain seems to somehow "saturate".

There are two reasons for this: the resonant system and the observer. Fig. 4(d) shows the simulation results when the observer is omitted and Ω_1 from the three-inertia plant model is connected directly to the controller's actual speed input. There is a considerable approximation to the ideal case, which is marked by (e), simulated with the observer neglected and the plant model reduced to a single inertia.

This "saturation" is the reason why the strongly increased controller gain using observers does not result in an appropriate rise of dynamic stiffness (fig. 9).

V. Speed Quality vs. Controller Gain

Speed errors at steady state are caused by errors in the sensor signals, which are amplified by the control and applied to the drive as current, causing energy consumption and real deviations. In addition, the weakly damped resonant poles of the system move towards the instable region when the controller gain is raised.

Fig. 5 shows the relationship between controller gain, speed quality and motor current. The data were measured on the setup using different PI speed control with 1st order filters to acquire the actual speed signal from the 5000-line encoder's position signal. There is a optimum around controller gain 1000 where the speed deviation is minimal. For higher gains, both deviation and current are raised dramatically, because the plant's resonance is excited; this is also clearly audible. With lower gains, the deviation rises also, this time because of disturbance forces caused by slot latching; the controller cannot properly compensate them because of its large phase lag. The chosen deviation of 0.7 rad/s is at the upper limit of a sensible control;

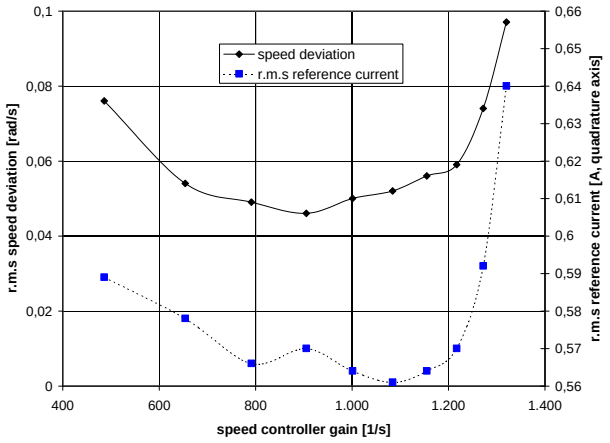

Fig. 5. Experimental results for r.m.s speed error deviation in steady-state regime vs. controller gain

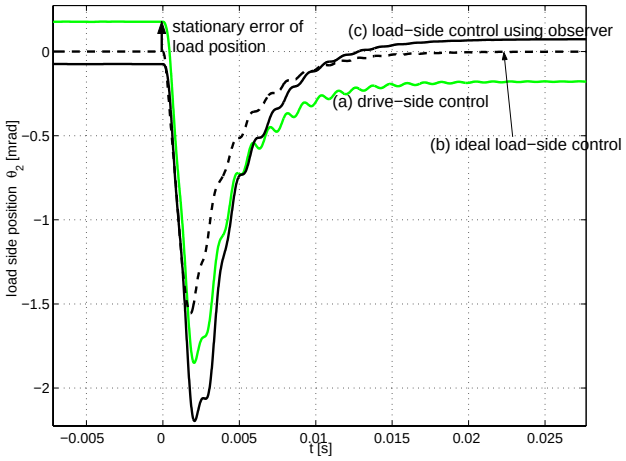

Fig. 6. Simulation of drive-side and load-side position control, 3-inertia observer and P/PI-cascade

above this point, the resonance is audible, and the position control loses stability.

VI. Static Stiffness

As the three-inertia model already suggests, the plant has elastic couplings between the components and thus a limited static stiffness. It can be measured if one servo is position-controlled while the other applies a defined load torque; then, the position measurements at drive and load can be compared. Measurements at different loads in the motor's torque range suggest an static stiffness of 12107 Nm/rad, and no measurable backlash. Though this should be equal to the spring constant c_{12} in the three-inertia model (table I), it differs quite a lot. The reason is that the models were optimized to mirror the plant's resonant behavior, and not the static one; the exact plant model is of much higher order. The stiffness computed from the coupling's datasheet was even less precise.

The effect of the limited stiffness is visible in fig. 6. Graph (a) shows the load-side position during position control with reference position 0. The load torque changes at $t = 0$ from +50% to -50% nom. torque. Though the drive is controlled to zero deviation, the load-side position has a considerable error due to the plant's limited stiffness. It is an interesting fact that though the plant regarded is a direct drive, the stationary position error is a relevant part of the dynamic deviation during load changes. In [2], this effect was neglected, thus the reported dynamic stiffness values were considerably higher.

The plant has an encoder fixed on the load servo, however, its precision is lower and the signals are considerably noisy. Thus, the best way to compute the load-side dynamic stiffness was to measure the drive-side deviation and add the stationary error. In simulation, an adapted model was used where c_{12} equals 12107 Nm/rad. This model is less precise than the original model concerning the frequency response. However, it simulates the static deviation correctly.

This problem leads to the idea of compensating the load position error, which can be achieved by load-side control. This means that the position controller and the integral part of the speed controller work on the load-side actual values. The proportional part of the speed controller must stay working on drive-side speed, because it would excite the resonance between drive and load otherwise. A simulation using this structure is shown in fig. 6(b). A three-inertia observer is used to compute the actual speed for the proportional speed controller, while integral speed controller and position controller use the directly acquired load-side speed and position. In comparison to the drive-side case, the new structure does not only compensate the steady-state position deviation, but also improves the dynamic stiffness. The reason is that a load change affects the load speed earlier than the drive speed; thus the load-side control will counteract earlier.

However, if a load-side encoder is not available, an observer must be used to determine the load-side position and speed. In fig. 6(c), the simulation result is shown when the speed controller's integral part uses the observed load speed, and the position controller uses

$$\hat{\theta}_2 = \theta_0 - \frac{T_{12}}{c_{12}} \tag{4}$$

as an actual position estimate. For c_{12}, the exact value has been used; the three-inertia observer estimates the spring torque T_{12}. It works with the model parameters shown in table I, therefore the steady-state deviation cannot be exactly compensated. The dynamic performance has even been worsened by this structure. The reason is that there is a positive static deviation before the load change in case of the drive-side control, which increases the level of the whole graph, thus reducing the negative deviation. The observer is not fast enough to compensate for this disadvantage before the maximum deviation point.

The static compensation might be useful in applications where the steady-state deviation is of interest. However, as in this paper the focus is on dynamic stiffness and the load-side encoder shall not be used, it is not capable of improving performance.

VII. Experimental Results using Filters and Observers

The following sections compare different speed computation methods concerning their influence on control

performance.

The standard method for industrial drives is using the low-pass filtered derivative of the position signal as speed feedback. For the investigated setup, main task for the filter was to passively damp the resonant frequencies in order to allow high controller gains. IIR filters derived from 1st order differentiating low-pass filters yielded the best performance [2].

To passively damp the resonant frequencies, one or two notch filters can be used. They are designed independently and then cascaded to the low-pass by multiplication of the transfer functions. Standard notch filters are achieved from the lowpass-to-bandstop transformation of first order lowpass filters. As time constant of the filter, which is needed for controller design, the first order approximation of the transfer function's denominator (in time-continuous domain) was used. It was modified by varying the cutoff frequency of the low pass filter; the notch filters turned out to contribute only a small phase lag.

An alternative to deal with the mechanical resonance is the use of an observer that models the mechanical system.

The models used are shown in fig. 2. Modeling only the encoder resonance (fig. 2(a)) is already quite a good model. For a three-mass approach, sensor, controlled servo and load servo are modeled as three inertias, joined by elastic couplings (fig. 2(b) and fig. 7).

The procedure of model identification is described by Mueller [8]: A multi-sine signal is used to excite the system; then the poles and zeros are visible in the FFT of the derived position signal. The models are designed to mirror the lowest critical frequencies identified. The resonant frequency with 5000-line encoder is lower because, with changing the encoders, the acceleration sensor's aluminium disc was exchanged for a brass disk; this increased the inertia.

The three-inertia model used for observation differs in some ways from the simulation model. The system was modeled undamped to reduce its complexity. An integrator is estimating the load torque, which was modeled as affecting all inertias equally. This is not physically correct, but decouples the load torque observer from system oscillations, improving observer performance. The proportional part of the PI speed controller was implied in the system model as if it was part of the system; this path is depicted as a dashed line in fig. 7. The two inertia model is constructed by leaving out the paths containing c_{12} and J_2.

The observers were designed similarly to [9], [4]: The position angle is derived and compared to the modeled encoder speed $\hat{\Omega}_0$, the difference is used for feedback. Other structures are possible, but yielded inferior results [2].

For feedback design, the method of eigenvalue placing was used. The original systems have two poles at s = 0 and one or two pole pairs (two or three inertia model, respectively) that represent the resonance. The resonant poles were moved to the left, leaving their imaginary part nearly constant. The eigenvalue at zero was moved far to the left to -3000 rad/s. Table I shows the system parameters and pole configurations used. In order to tune the control loop for the given speed quality of 0.1 rad/s,

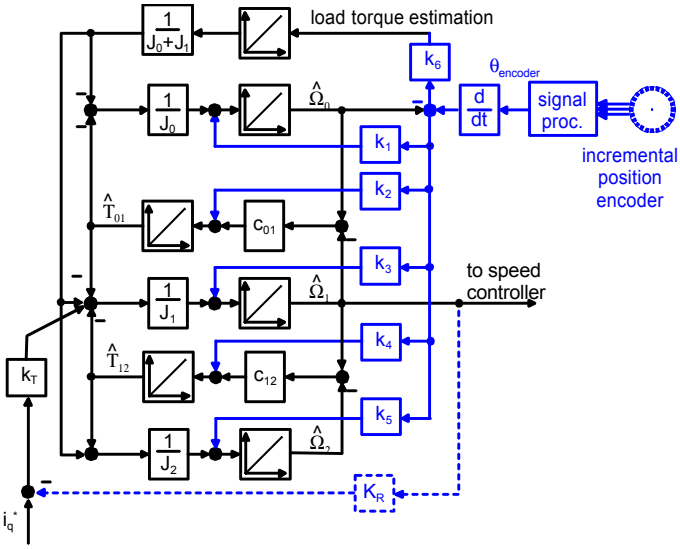

Fig. 7. Structure of the three inertia system model (parameters see table I

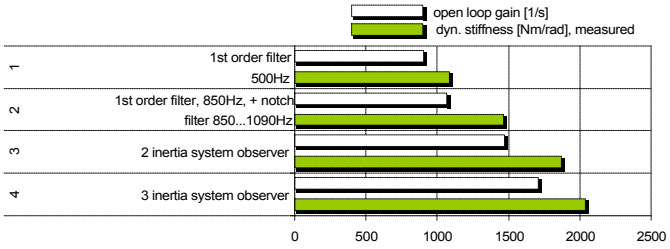

Fig. 8. Experimental and simulation results using 2048-line encoder

only the PI controller gain was changed.

Fig. 8 presents the results measured with the 2048-line encoder. All controls were tuned to achieve a r.m.s speed error of 0.1 rad/s at steady state in the experiment. Fig. 8 shows the final speed control loop gain and the dynamic stiffness. The stiffness was measured changing the load servo's current reference value while the drive was position-controlled. In addition, the simulated dynamic stiffness is shown. Simulation is in two ways more precise than measurement:

- The simulation was done for a stepwise load torque change instead of the load servo controller's response function, because this is the usual definition of dynamic stiffness. This might shrink the stiffness because it is a faster change, and moreover might cause overshoots of position deviation due to the resonant frequencies, because an ideal step function has a larger high-frequency content and is more likely to excite oscillation.
- The measured encoder angle is the drive-side encoder readout, because this encoder is much more precise. The static deviation was added. The simulated dynamic stiffness is computed using the load-side position deviation; this includes the oscillation behavior which might either increase or shrink the deviation.

Fig. 8 illustrates a clear ranking: Compared to the low-pass filter, the low pass plus notch filters (fig. 8 no.2,

TABLE I

IDENTIFIED SYSTEM PARAMETERS AND POLES USED

	J_0 kgcm^2	J_1 kgcm^2	J_2 kgcm^2	c_{01} Nm/rad	c_{12} Nm/rad	pole(s) Hz	zero Hz	observer poles rad/s
2-inertia system, 2048-line encoder	2.7	17.35		8679		970		$-1881 \pm j5168$ -3000, -3000
3-inertia system, 2048-line encoder	2.09	8.7	9.26	10376	22249	970, 1370	780	$-1881 \pm j5168$, $-1562 \pm j8863$, -3000, -3000
2-inertia system, 5000-line encoder	2.8	17.25		7214		870		$-1710 \pm j4700$ -3000, -3000
3-inertia system, 5000-line encoder	3.1	8.4	8.55	11100	19600	872, 1286	762	$-1710 \pm j4700$, $-1562 \pm j8863$, -3000, -5000
Simulation model (3-inertia system, 5000-line encoder)	2.07	12.71	5.27	11156 $d_{01} = 0.045$	12107 $d_{12} = 0.14$	870, 1285	762	

fig. 9 no.2,3) perform significantly better. The reason is that the notch filter achieves a much better suppression of the resonant frequencies, while contributing only few to the delay time constant.

The observers for two and three inertia systems (fig. 8 no.3,4, fig. 9 no.4,5) implement knowledge about the mechanical resonance in a physically quite correct way. As a result, their performance is significantly better than that of a filter. Best performance is achieved using the three mass system observer, because this is the most precise model. However, it must be added that the three-inertia model is much more complicated to identify and depends on the load servo inertia, which the two-inertia model does hardly; since J_0 is much smaller that J_1, the resonant frequency is mainly determined by J_0.

Hardly any difference can be seen between the simulated and measured dynamic stiffness. This means that the slope of the load servo's current control is steep enough to simulate a stepwise load change. Regarding the graph of position during a load torque change shown in fig. 6, it can be seen that mechanical resonance does not play a mayor part in position deviation, and that the whole process is rather slow compared to the load servo's rise time of 500 μs.

VIII. EXPERIMENTAL RESULTS USING DIFFERENT ENCODERS

Fig. 9 shows measurements using some of the filters with the 5000-line encoder. Again, the diagram shows that the performance using a 1st order filter -which is already quite good- can be improved using notch filters. Because of the higher control loop bandwidth, a double notch filter could again improve performance, which was not the case with the 2048-line encoder.

A comparison with fig. 8 shows that the filter controls profit from the better position signal - though the speed error limit has been reduced. This is due to the fact that the resonant frequencies are excited by speed signal noise times filter gain at the respective frequency times controller gain. If the speed noise is reduced, the filter gain a the resonant frequency may be higher without exciting the plant above its passive damping capability.

The observers for two and three inertia systems achieve nearly the same results as with the 2048-line encoder; they do not profit from the better position signal. This indicates that an observer-based control does not depend as much on sensor quality as a filter-based control does. The explanation is that an observer is a system of much higher order than a filter. Though feed-forward signals can pass it directly, feedback signals are delayed and smoothed in the feedback path. As the observers use a quite precise model and low feedback constants, the transfer function from encoder signal disturbances to $\hat{\Omega}_1$ has a low magnitude, especially at high frequencies where differentiation noise becomes critical.

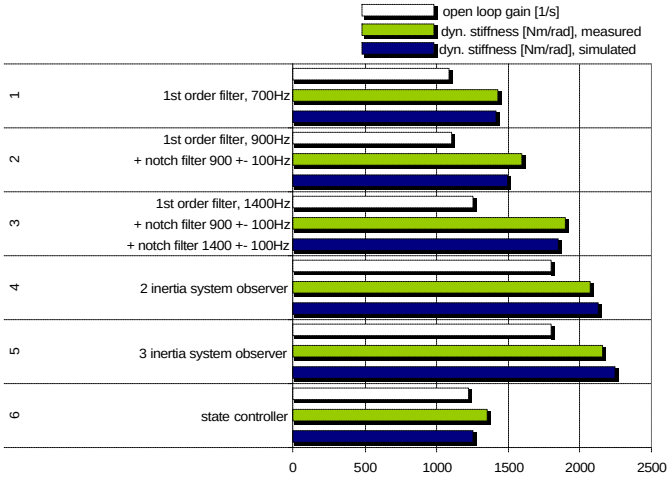

Fig. 9. Experimental and simulation results using 5000-line encoder

Though there there is a considerable difference in controller gain between the double notch filter (no. 3) and the observers, the improvement in terms of dynamic stiffness is only small. The reason is the "saturation" effect discussed in section IV.

IX. THE INFLUENCE OF CONTROLLER TIMING

The measurements shown in section VII were done using a digital control with a timing of 100 μs sampling time and 40 μs calculation time between A/D and D/A conversion. This timing was used for the position and speed control; the current controller works continuously. The following table shows measurements at a timing of 26.25 μs, which is the fastest possible at the setup. The 5000-line sensor has been used.

The observer's feedback was again designed by pole placing. The pole locations used are shown in table II. They resemble the pole locations used at slower timing,

TABLE II

POLE LOCATIONS FOR OBSERVERS AT FASTER TIMING

	observer poles [rad/s]
2 inertia system observer	$-3210 \pm j3830$, -3000, -3000
3 inertia system observer	$-1165 \pm j4350$, $-1390 \pm j7880$, -3000, -3000

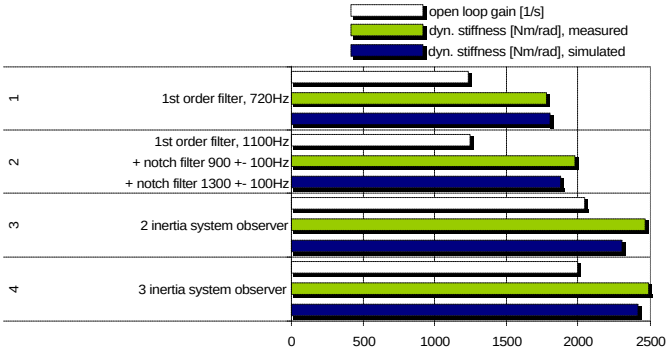

Fig. 10. Experimental and simulation results using fast sampling rate

except that the poles of the two inertia observer had to be damped stronger. This is because the 2-inertia model is less precise, thus it needs a stronger feedback from the sensor to keep the estimated values close to the real ones.

Fig. 10 shows the achieved stiffness at faster timing, showing again the same ranking as in figs. 8 and 9. The achieved stiffness is much higher than at slower timing, though the used cutoff frequencies and controller gains have not changed much. This is simply due to the fact that the control can react faster to a deviation, limiting the acceleration caused by the load step change.

X. ACTIVE DAMPING

Fassnacht [9], [4] reported that active damping of a three-inertia plant is possible using only a PI controller. This is also true for the setup regarded here, however the achievable damping is much lower; and it is necessary to use the motor speed rather that the sensor speed. As opposed to the standard case, sensor and actuator of the plant regarded here represent different inertias. At the oscillation frequency, these two masses will oscillate against each other. If speed is measured on one of them and fed back to the other, the oscillation will be excited instead of damped. Fig. 11 shows the root locus plot when Ω_1 is fed back to motor current by a p-controller with a deadtime of 90 μs (3rd order Pade approximation). The achievable damping for the lower resonant frequency, which is dominant in practice, is very poor: the optimum pole location is $-630 \pm j5250$ rad/s, meaning a 5% settling time of 4.7 ms, at a gain which cannot be achieved in practice.

A better active damping is only possible using a state controller. The state controller was designed by pole placing, shifting the resonant poles directly to the left as it was proposed by Goslar [3]. The pole pair representing the lower resonance frequency was moved towards the left by 1710 rad/s, the pole pair for the upper resonance was nearly left in place as this frequency does not appear in the measurements. The pole at zero is moved to the

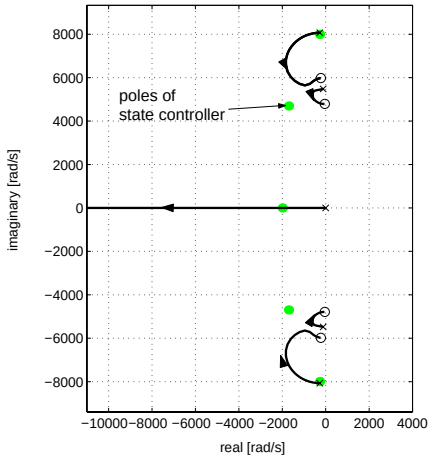

Fig. 11. Root locus graph for proportional feedback of Ω_1

TABLE III

POLE LOCATIONS OF STATE CONTROLLER AND OBSERVER

	poles [rad/s]
state controller	$-1710 \pm j4700$, $-300 \pm j8000$, -2000
observer	$-255 \pm j4560$, $-1970 \pm j8064$, -3900, -3000

left; its position determines how fast the controller will be. Table III shows the pole locations that were used for state controller and observer, the state controller's poles are also shown in fig. 11.

The observer design is much more complicated than it was for the PI control. The final solution was an observer whose resonant poles are not much faster than the state controller's; the pole pair representing the lower resonance frequency is slower, i. e. further to the right. Pole patterns with faster observer poles would cause oscillations even at steady state, or require a controller design with less damping. The used pattern means that concerning the oscillations, the observer relies on its model rather than sensor feedback. Only the overall speed and load torque are observed with much faster time constants than the state controller's.

The reference value is fed into the state control system by a proportional prefilter [10]. The prefilter constant was regarded as the proportional gain K_R, then integration time constant and position controller gain were chosen appropriately. This way, a PI-state controller [10] was designed that replaces the PI speed controller and can be cascaded with a proportional position controller - this ensures comparability with the previous designs.

Fig. 9 no. 6 shows that the dynamic stiffness of the state controller is only in the range of a filter control. It cannot be raised further because of the steady-state performance required. This is the price for active damping: it does not contribute to dynamic stiffness, but creates inquietude in the control system, thus reducing the allowable controller gain.

The effect of active damping is seen best regarding a stepwise setpoint change of the speed control [9]. Fig. 12 shows measured graphs of reference current i_q^* and encoder speed Ω_0 using different controls. The reference step

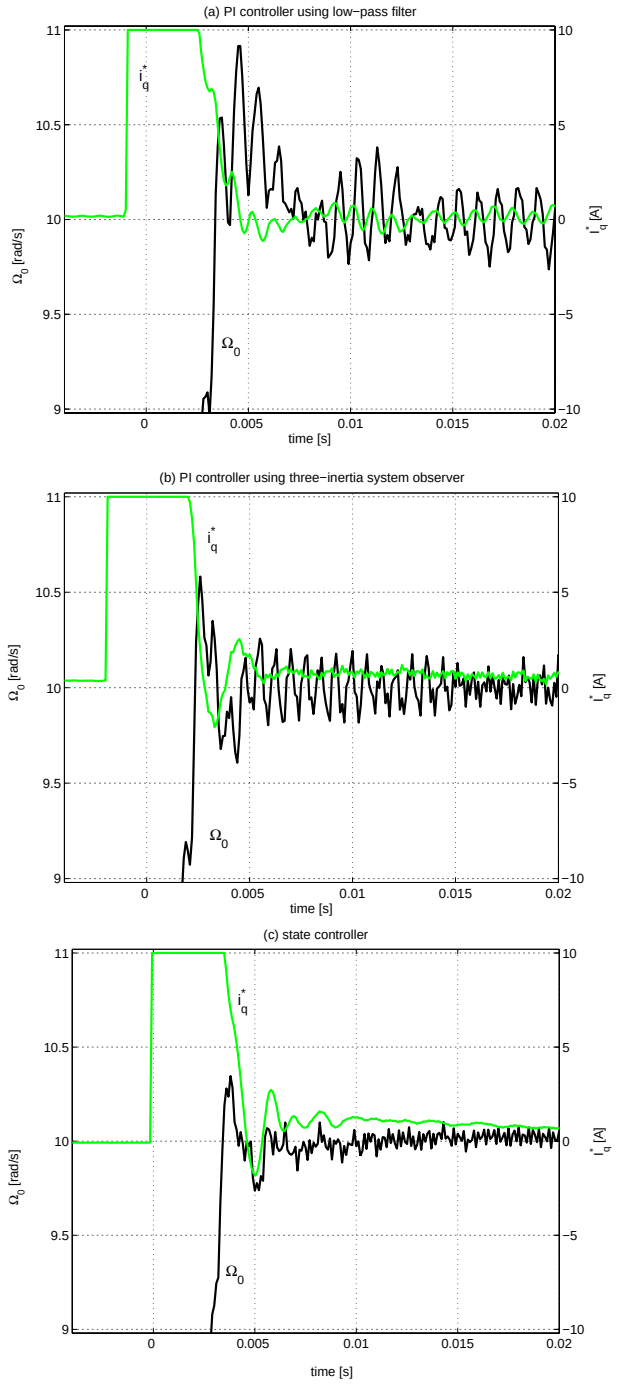

Fig. 12. Setpoint change during speed control; experimental results

excites the plant's resonant frequencies, and the current limit prevents damping by the controller. As soon as the current limit is left, damping starts. Fig. 12(c) shows that the state controller is able to damp out the oscillation within two periods. The PI controller using an observer (fig. 12(b) provides a weak active damping, while the PI control using a filter does not damp the oscillations at all (fig. 12(a)).

XI. Conclusion

Starting from theoretical considerations, it was shown that the delay of speed acquisition and the plant resonance play an important part for the reachable dynamic stiffness, not only indirectly because they limit the controller gain, but also directly. With highly dynamic controls, there is only a small improvement of dynamic stiffness because performance is limited by the resonant system and observer delay. The graph of steady-state speed error in terms of controller gain shows that there is an optimal gain. Even for direct drives, the limited static stiffness of the plant reduces the achievable dynamic stiffness. However, a sensible compensation of that effect is only possible if a load-side encoder is available for control.

Different speed computation schemes to provide the actual speed signal for a cascade control were investigated. Keeping the steady-state behavior equal, it was shown that the stiffness against load changes can be improved using notch filters, and further using observers modeling the plant's resonant behavior. The approximation of the plant as either a two or a three inertia system works nearly equally well, while the two inertia model is of lower order and easier to identify. Active damping cannot be done by the PI controller, but using a state controller. However, the price for active damping is a reduction of control gain, resulting in a reduction of dynamic stiffness.

The comparison of results with different sensors revealed that a control using filters is strongly dependent on the encoder signal quality. Using an observer, the performance is quite independent from the signal quality; therefore, cheaper sensors can be used. At a faster control timing, the allowable gain with respect to the steady-state performance requirements is approximately the same. Anyway, a significantly better dynamic stiffness is possible.

Acknowledgment

This paper presents results of research project MU 1109/6-2, supported by the DFG Deutsche Forschungsgemeinschaft.

References

[1] M. Weck, P. Krueger, Ch. Brecher, F. Remy: *Statische und dynamische Steifigkeit von linearen Direktantrieben*; Antriebstechnik No. 12, Vol. 36 (Dec. 1997), pp. 57-63

[2] Baehr, A., Mutschler, P.: *Comparison of Speed Acquisition Methods based on Sinusoidal Encoder Signals*; Optim 2002, 16.05.-17.05., Brasov, Romania

[3] M. Goslar: *Ein Beitrag zur anwendungsorientierten Zustandsregelung elektrischer Hochleistungsantriebe*; PhD thesis, TU Clausthal 1998

[4] J. Fassnacht, *Schwingungsbedaempfung in Servosystemen mit der direkten Drehmomentmittelwertregelung*, PhD thesis 2002, available online at http://elib.tu-darmstadt.de/diss/000273/

[5] A. Baehr, P. Mutschler: *Systematic error correction methods for Sinusoidal Encoders and their Application in Servo Control*; EPE 2003, 03.09.-05.09., Toulouse, France; paper no. 266

[6] B. Hoescheler: *Innovative technique for easy high-resolution position acquisition with sinusoidal encoders*, IEEE proceedings on intelligent motion, june 1997, pp. 407-416

[7] M. Kazmierkowsky, A. Dzieniakowsky, W. Sulkowski: *Novel Space Vector Based Current Controllers for PWM-Inverters*; IEEE Transactions on Power Electronics Vol. 6 pp. 158-165, January 1991

[8] Mueller, I.: *Two Reliable Methods for Estimating the Mechanical Parameters of a Rotating Three-Inertia System*; EPE - PEMC 2002, 09.09.-11.09., Dubrovnik, Croatia;

[9] J. Fassnacht, P. Mutschler: *Benefits and Limits of Using an Acceleration Sensor in Actively Damping High Frequent Mechanical Oscillations*; 36th IAS Annual Meeting in Chicago 2001, Conference Record pp. 2337-2344

[10] O. Foellinger: *Regelungstechnik*; 8. Auflage, Huethig Buchverlag 1994